

Evaluation of SCAA Mask Technology as a Pathway to the 65 nm Node

James V. Beach*^a, John S. Petersen^b, Mark J. Maslow^b, Dave J. Gerold^b
and Diane McCafferty^c

^a International SEMATECH, Austin, TX 78741,

^bPetersen Advanced Lithography, Inc., Austin, TX 78750

^cASML, Wilton, CT 06897

ABSTRACT

This study takes an integrated approach utilizing a combination of high NA 193 nm lithography, a sidewall chrome alternating aperture (SCAA) phase shift mask, optical proximity correction (OPC) and customized illumination in an attempt to demonstrate the feasibility of using 193 nm lithography to support the 65 nm node. A SCAA mask was designed and built with line/space patterns ranging in pitch from 300 nm down to 140 nm. A range of mask biases were applied to the zero and pi spaces in order to examine to response of the lithography to a combination of the SCAA approach and asymmetric biasing. In combination to the asymmetric biasing, overlay bracketing was applied in order to measure the chrome overlay tolerances of the mask. Simulations suggested that an unconventionally small sigma of 0.15 would be the optimum coherence for a high 193 nm optical system. A custom 0.15 sigma partial coherence illuminator was, therefore, built and installed in the experimental ASML Micrascan V 0.75 NA 193 nm scanner.

Wafers were exposed using 190 nm of 193 nm resist and an organic BARC. The 70 nm 1:1 line/space patterns resolved with a depth of focus of about 0.2 μm . The 75 nm 1:1 line/space patterns showed a 0.3-0.4 μm depth of focus. Both of these process windows were limited by pattern collapse. Addressing the pattern collapse may improve the depth of focus. Comparing mask measurements to wafer measurements show that little or no asymmetric biasing is necessary to balance the pitch. Moreover, the measured pitch was stable over a focus range of at least 0.4 microns demonstrating that any phase imbalance present was not significantly affecting the observed lithography.

INTRODUCTION

At its conception, 193 nm lithography was thought to be the best way to take optical lithography to the 180 nm node. Today, 193 nm must compete with 248 nm for the 130 nm node and is expected to support lithography until it is replaced by 157 nm at the 65 nm node. Given the challenges facing 157 nm, it is likely that lithographers will attempt to extend the utility of 193 nm to its theoretical limits.

The first production-ready 193 nm scanners had a maximum numeric aperture (NA) of 0.75. Newer tools will have NAs of 0.80 to 0.85 to something higher (There is now even talk of immersion lithography with NAs greater than 1.0¹). In order for 193 nm technology to achieve the 65 nm node, lithographers will have to operate at very low k_1 (Table 1).

NA	90 nm k_1	65 nm k_1
0.75	0.35	0.25
0.85	0.40	0.29
0.93	0.43	0.31
1.3	0.61	0.44

Table 1. Calculated k_1 values (Rayleigh equation) for 193 nm lithography operating at the 90 nm and the 65 nm nodes.

*james.beach@sematech.org; phone (512) 356-3737

Aggressive optical extension techniques will be necessary in order to drive 193 nm to the 65 nm node. Marc Levenson's sidewall chrome alternating aperture mask (SCAA) has proven in theory to be a superior approach in terms of controlling transmission and phase imbalance in alternating aperture phase shift masks^{2,3}. Of particular importance is its insensitivity to mask sidewall profiles. As the feature sizes begin to challenge the mask maker's abilities and the aspect ratio of the etched glass trench increases (almost 1:1 for a 65 nm line at 193 nm) control of the mask sidewalls will be difficult. Because of this, we selected SCAA as the most appropriate approach for this study despite its current manufacturing issues. This study takes an integrated approach utilizing a combination of high NA 193 nm lithography, SCAA phase shift mask, OPC and customized illumination in an attempt to demonstrate the feasibility of using 193 nm lithography to support the 65 nm node. Since this study will utilize a 0.75 NA 193 nm scanner, the minimum pitch attempted was 140 nm ($k_1 = 0.27$). The results then can be extrapolated to 130 nm with higher NA.

APPROACH

The exposure tool for this work has a maximum numerical aperture of 0.75. Since the sigma space (the Fourier plane) places the diffraction orders at:

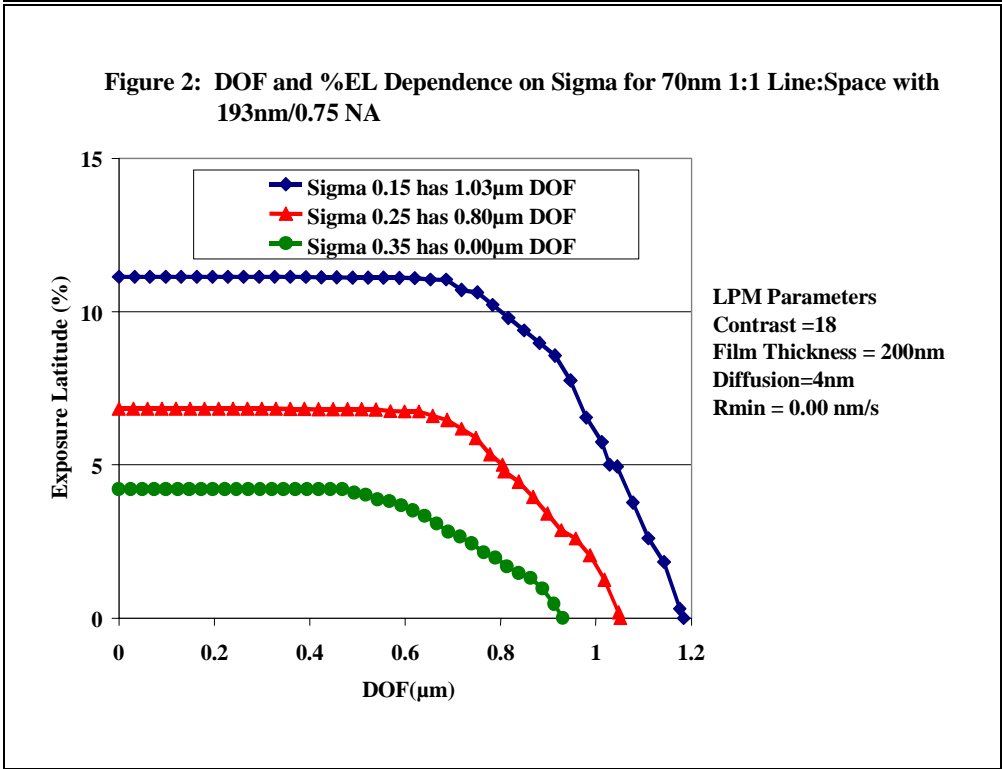
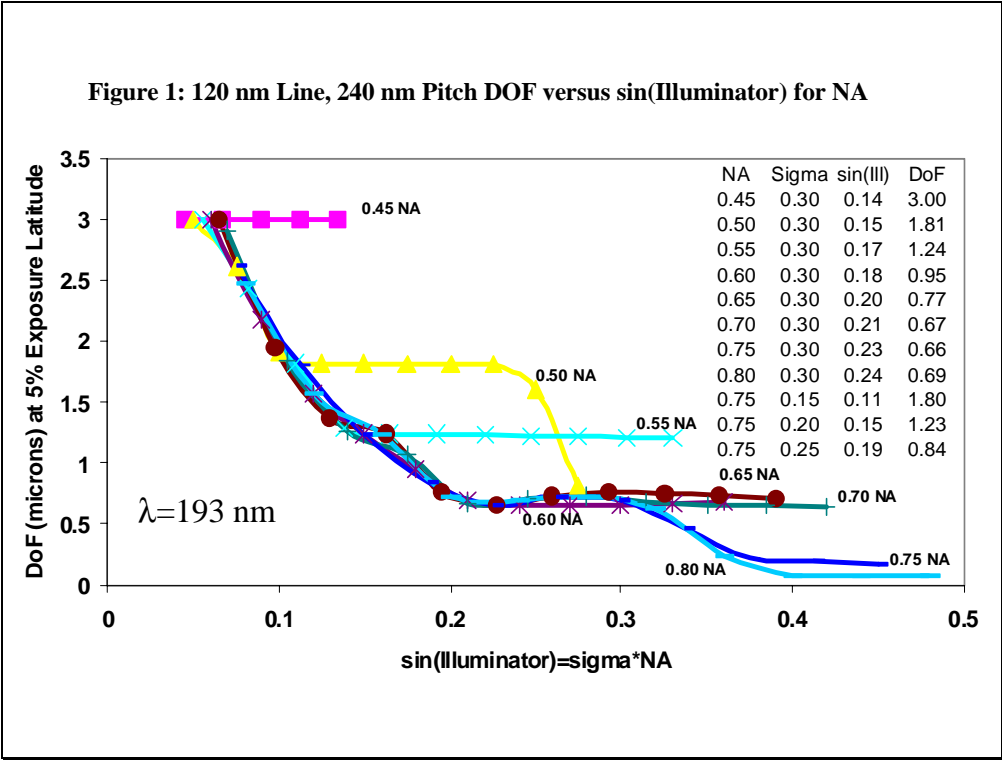
$$\sigma_{\pm 1\text{st-order}} = \lambda \cdot (2 \cdot \text{Pitch} \cdot \text{NA})^{-1} = 193\text{nm} \cdot (2 \cdot 140\text{nm} \cdot 0.75)^{-1} = 0.92$$

the diffraction orders are at the very edge of the pupil. For strong phase shifting, the best results occur with a high degree of coherence. Historically, a value of 0.3 to 0.45 is the typical sigma value chosen for strong PSM applications. However, it has been observed that depth of focus (DOF) decreases with increasing numerical aperture, which for the casual lithographer is assumed to be related to the Rayleigh criterion = $\text{DOF} = k_2 \lambda / \text{NA}^2$. However, this relationship does not hold for two-beam imaging, which is in phase as long as spatial and temporal coherence are maintained. In addition, the loss of DOF shown in Figure 1 shows for the same diffraction pattern, in this case a 120nm equal line-space, that DOF decreases with increasing NA. The reason for this lies in the definition of partial coherence,

$$\sigma = \sin(\text{illuminator half cone angle}) / \text{numerical aperture}$$

Thus with increasing NA, the $\sin(\text{illuminator})$ must increase to maintain a constant sigma value. Increasing illuminator angle decreases symmetry of the interference about the optical axis and this loss of symmetry induces a phase error in the presence of an aberration such as defocus. As Figure 1 shows, increasing illuminator angle decreases DOF. Thus, due to the difference in illumination angle, it makes no sense to use 0.3 sigma at 0.45NA and 0.75NA. It is better to fix the illumination angle and let sigma change. For the 70nm node, we found that a good sigma would be 0.15. This is shown in Figure 2, which compares process windows at 0.15 and 0.25 sigma values for 45nm lines and 140nm pitch, and shows that the lower value, sigma of 0.15, is superior.

A custom 0.15 sigma illuminator was created for this experiment and installed in the scanner. All exposures reported in this study used this custom aperture.



Figures 1 and 2. Optimization of illumination conditions for high NA.

MASK

A SCAA mask was designed and built by the authors using EMF simulations, CAD by Benchmark Technologies and fabrication by Dai Nippon Printing. The mask has a large number of line/space patterns ranging in pitch from 300 nm down to 140 nm. A range of mask biases were applied to the 0 and pi spaces in order to examine the response of the lithography to a combination of the SCAA approach and asymmetric biasing. In combination to the asymmetric biasing, overlay bracketing was applied in order to measure the chrome overlay tolerances of the mask.

Inspection showed the chrome lines to be undersized by about 5% but showed good linearity through size and pitch. Phase measurements came in at 182° with a range of 2.5° across six measurements (Table 2).

	Mean	Std.
CD Target		
160 nm	147 nm	
240 nm	229 nm	3.4
360 nm	346 nm	
Phase	182°	0.8

Table 2. Mask metrology data for mask CDs and phase.

Several sets of lines were created at each pitch to determine if an asymmetric bias was necessary for the SCAA approach. Figure 3 shows the application of the biasing. The pi space only was biased while leaving the zero space constant. Note that this approach will make the chrome line larger as the space becomes smaller.

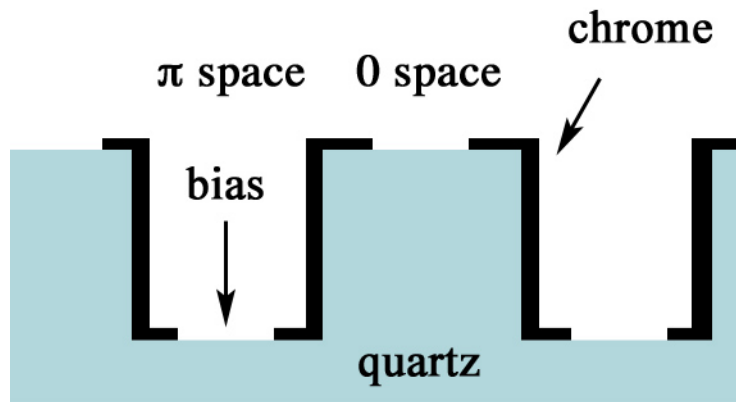


Figure 3. Biasing of the SCAA mask.

Top down measurements of the mask were made in order to understand any etch bias that may exist during mask fabrication between the zero and pi space. Table 3 shows the empirical mask measurements vs. the applied bias to the GDS data. The table shows that a small bias (20-30 nm in mask dimensions) is necessary in order to balance the zero and pi spaces on the mask.

Pitch	target π space (nm)	target 0 space (nm)	mask bias (nm)	observed π space (nm)	observed 0 space (nm)	observed bias (nm)
160 nm	355	360	-5	402	383	19
	350	360	-10	395	386	9
	345	360	-15	389	386	3
	340	360	-20	383	386	-3
	335	360	-25	377	386	-9
	330	360	-30	371	380	-9
	325	360	-35	364	386	-22
	320	360	-40	361	380	-19
150 nm	355	355	0	401	380	21
	350	355	-5	397	380	17
	345	355	-10	388	380	8
	340	355	-15	384	376	8
	335	355	-20	388	384	4
	330	355	-25	372	380	-8
	325	355	-30	371	384	-13
	320	355	-35	363	376	-13
	315	355	-40	359	375	-16
140 nm	380	380	0	433	411	22
	375	380	-5	430	411	19
	370	380	-10	417	408	9
	365	380	-15	411	411	0
	360	380	-20	408	411	-3
	355	380	-25	404	411	-7
	350	380	-30	399	408	-7
	345	380	-35	396	411	-15
	340	380	-40	392	414	-22

Table 3. Measured mask biases for the pi and zero spaces (mask dimensions).

RESULTS AND DISCUSSION

All wafers (bare silicon) were coated with an organic BARC then 190 nm of ArF resist. The wafers were exposed with the experimental ASML Micrascan V 0.75 NA 193 nm scanner using a 0.15 sigma partial coherence followed by a standard PEB and aqueous develop.

The pattern showed good resolution down to the minimum pitch of 140 nm (Figure 4). The primary failure observed was pattern collapse, which was more prevalent at higher exposures as the CDs approached 60 nm. The 150 nm and 160 nm pitches showed less pattern collapse though it was still very prevalent. Figure 5 shows the observed process windows for the 160, 150 and 140 nm pitches. The 140 nm pitch showed a small process window with about 0.2 μm DOF with a 5% exposure latitude. Addressing pattern collapse by thinning the resist or by the use of a special rinse⁴ should significantly improve this process window as the features did not appear to have troubles resolving at negative focus, just resisting collapse. Biasing was applied to the chrome line (50 nm in wafer dimensions) but it is unclear from our observations if such biasing was necessary. The mask has a large range of biasing and this bias happened to fit best on the focus/exposure matrixes shot. A rigorous comparisons of line biasing was not done. The 150 nm and 160 nm pitches showed much improved process windows which, again, could be related to the reduced pattern collapse at these larger pitches. The target chrome lines were 72 nm and 85 nm (wafer dimensions) respectively on these pitches. These two pitches showed a very wide exposure latitude as predicted by simulations. DOF was measured at 0.4 μm at a 10% exposure latitude.

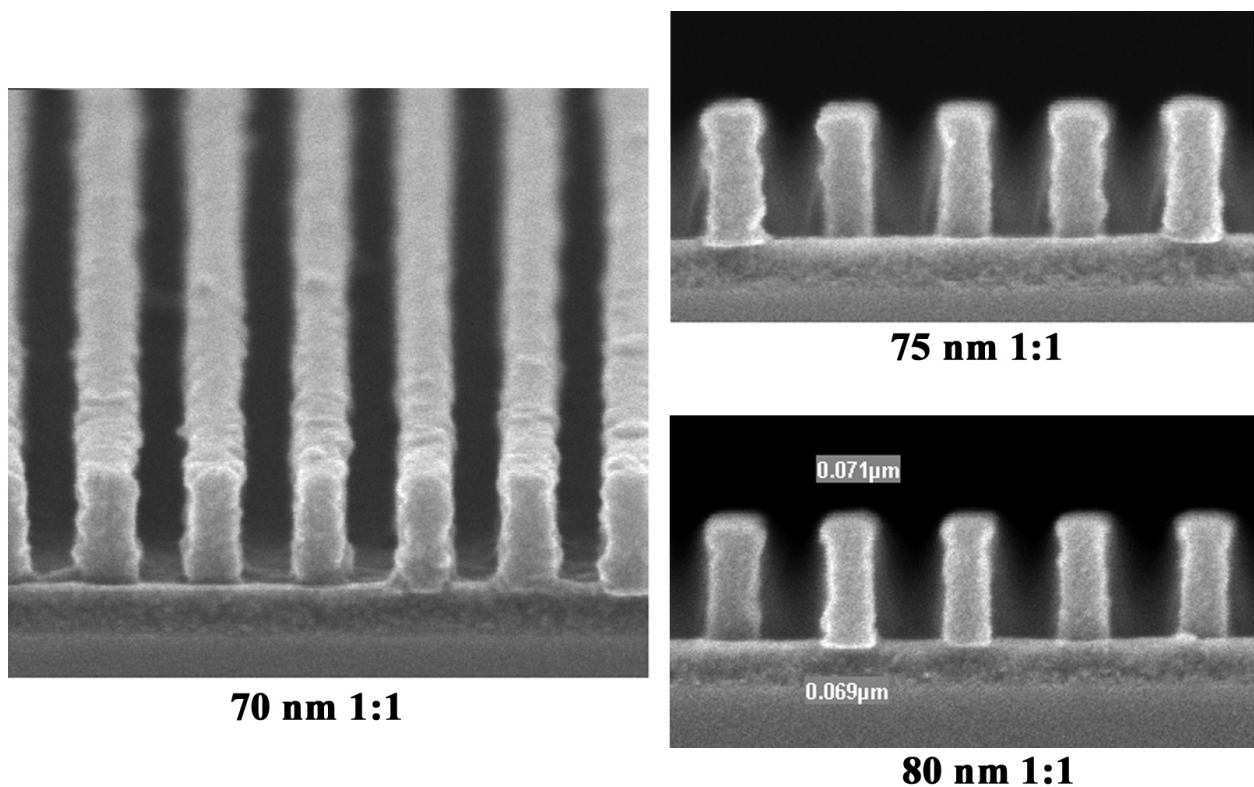


Figure 4. Cross sections of line features on a 140, 150 and 160 nm pitch

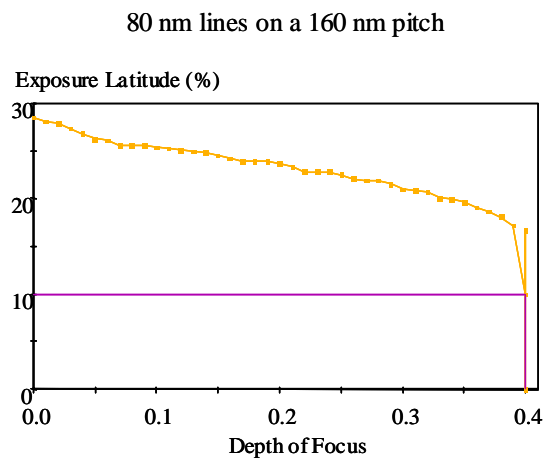
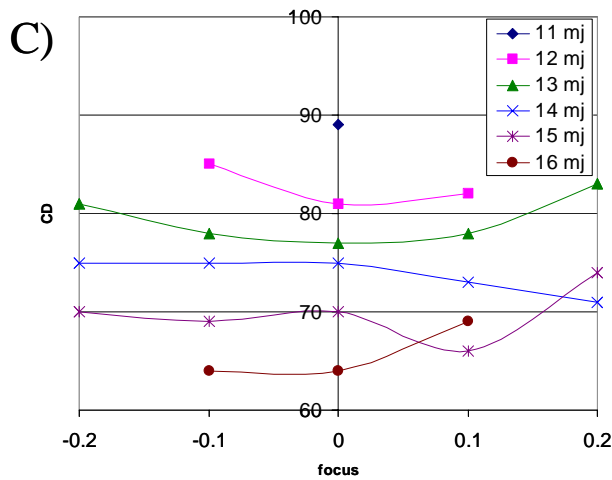
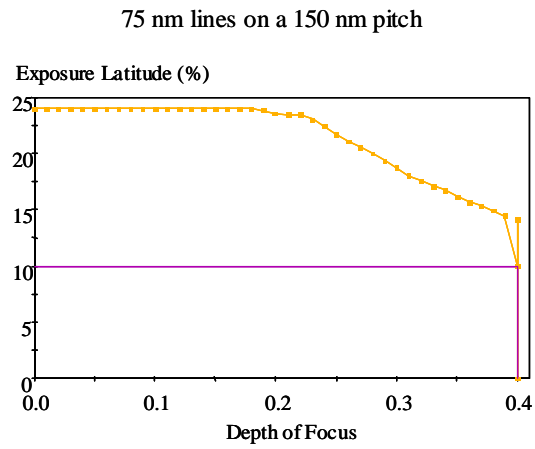
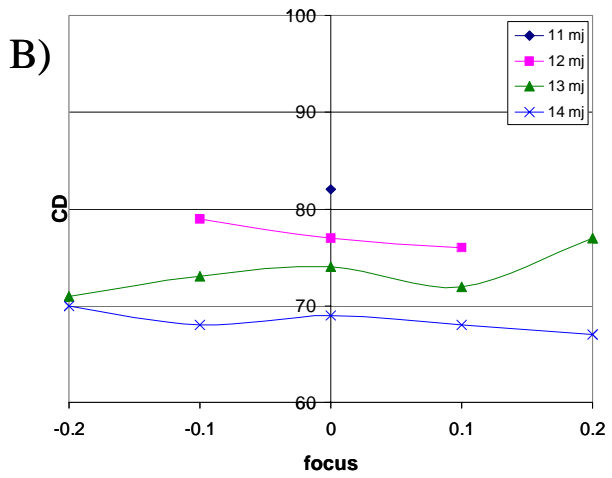
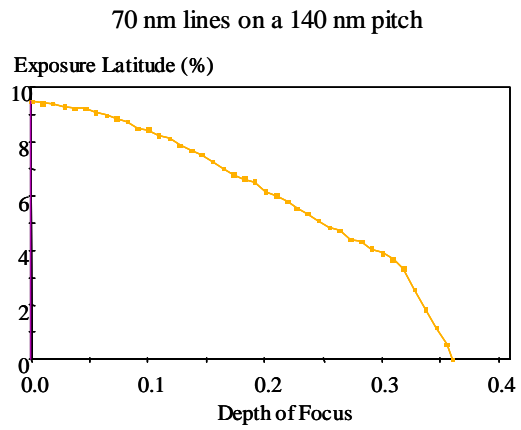
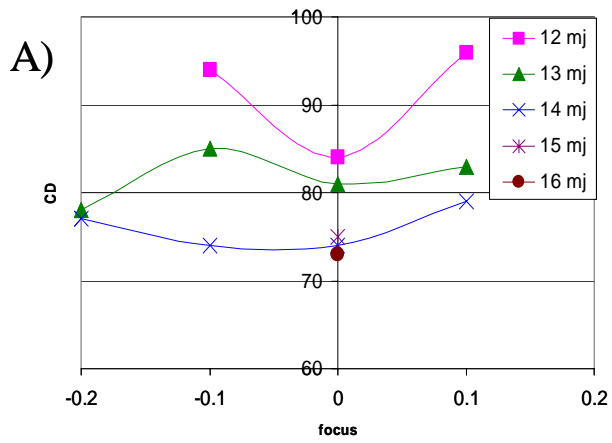


Figure 5. Process windows for dense line features. A) 70 nm lines on a 140 nm pitch. B) 75 nm lines on a 150 nm pitch. C) 80 nm lines on a 160 nm pitch.

Two pitches from three adjacent lines were measured on a top-down SEM through focus in order to determine the best biasing and to measure any phase imbalance present. Pitch imbalance tracked nicely with the observed mask bias suggesting little or no phase imbalance with the aerial image. The data is noisy as many of the patterns had severe pattern collapse which affected the data. Care was taken to make measurements only in areas a significant distance from the collapsed lines. Table 4 shows the data at best focus only. Treat the delta pitch numbers as absolute values as it was difficult to ensure that the same two pitches were measured in each case.

Pitch	observed pitch 1 (nm)	observed pitch 2 (nm)	delta pitch (observed) (nm)	target mask bias (nm)	observed mask bias (nm)
160 nm	158	162	4	-5	19
	157	163	6	-10	9
	159	162	3	-15	3
	159	160	1	-20	-3
	160	161	1	-25	-9
	159	160	1	-30	-9
	158	162	4	-35	-22
	158	161	3	-40	-19
150 nm	147	158	11	0	21
	148	157	9	-5	17
	149	154	5	-10	8
	150	154	4	-15	8
	151	154	3	-20	4
	151	152	1	-25	-8
	151	152	1	-30	-13
	152	152	0	-35	-13
	149	155	6	-40	-16
140 nm	---	---	---	0	22
	139	151	12	-5	19
	136	150	14	-10	9
	138	151	13	-15	0
	142	148	6	-20	-3
	140	148	8	-25	-7
	142	145	3	-30	-7
	144	144	0	-35	-15
142	146	4	-40	-22	

Table 4. Comparison of the observed pitch imbalance vs. the observed mask biasing (from Table 3).

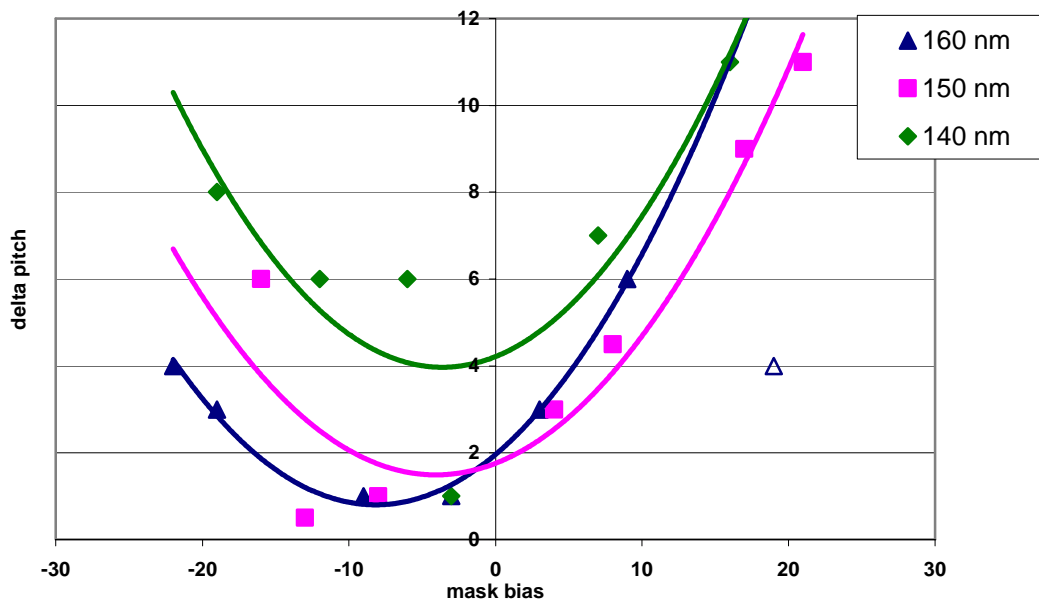


Figure 6. The measured mask bias versus the difference of two adjacent pitches measured on the wafer for the 160 nm, 150 nm and 140 nm pitch.

As mentioned earlier, the delta pitch numbers in Figure 6 were taken at the best focus. However, the measured pitches did not vary beyond experimental error through the entire range of measured focus regardless of the applied bias. Delta pitch numbers through focus are listed in Table 5. These results demonstrate a lack of phase imbalance with the SCAA mask approach.

Further evidence of this can be found in a chrome overlay study performed on the mask. A SCAA mask is not self-aligned and therefore requires second-level overlay. Theoretically, a SCAA mask would be insensitive to small errors in second-level overlay provided that the chrome edge does not encroach on the edge of the etched quartz. As the feature size shrinks, however, more accurate overlay becomes necessary to prevent this encroachment. For a 50 nm line, the quartz edge falls 100 nm from the chrome edge on the mask. Current mask tools can easily handle this requirement. It is not apparent, however, how close to this edge the chrome can get before sidewall effects begin to show.

Three modules were created with a +50 nm, 0 nm and a -50 nm overlay offset (mask dimensions). Figure 7 shows top-down SEMs of the mask for each of the three overlay brackets for the 140 nm and the 160 nm pitch. The features shown here are dark field lines. One can see that the center bracket is nicely aligned whereas the +50 and -50 brackets have chrome edges very close to the quartz edge. In the case of the 140 nm pitch, the edges appear to converge.

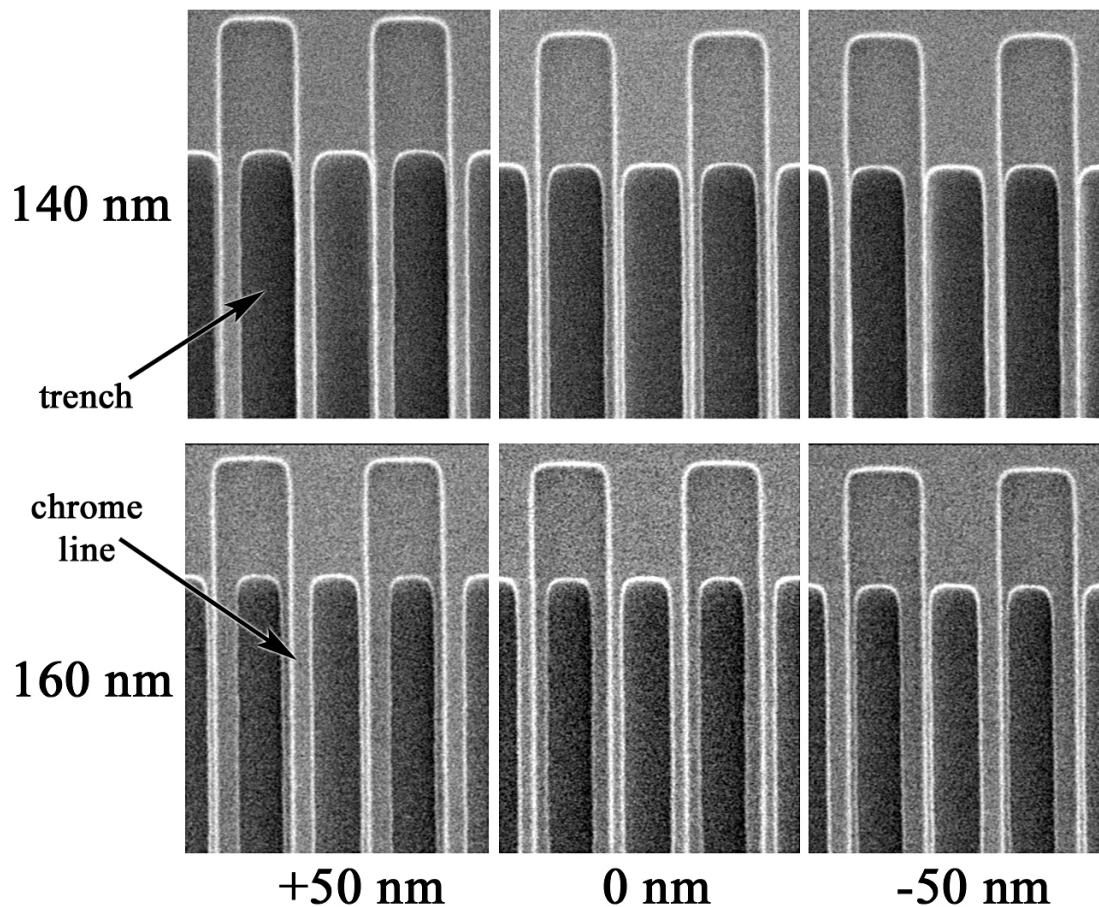


Figure 7. Top-down SEM pictures of the SCAA mask. Shown are the dark-field lines (140 nm and 160 nm pitch) with a +50 nm, 0 nm and -50 nm overlay bias.

Though more data needs to be taken, Table 5 (plus additional data not shown here) suggests pitch walking through focus for those features where the chrome edge converged on the quartz edge and stable lithography for those features where the edges had some separation. Hence, the 160 nm pitch showed consistent results through focus across all the overlay brackets. The 140 nm pitch, however, did show a dependency on the overlay. This dependency seems to be minimized as the pitch is balanced by mask biasing. Results from the 150 nm pitch were indecisive and will require a more detailed study. These results highlight the importance of second-level overlay for the very small lines (sub-60 nm) only.

target mask bias (nm)	overlay bracket (nm)	focus (μm)	delta pitch (nm)	
			140 nm	160 nm
-5	-50	0.1	collapsed	5
		0.0	8	7
		-0.1	19	8
		-0.2	collapsed	8
	0	0.1	collapsed	5
		0.0	14	4
		-0.1	17	4
		-0.2	collapsed	7
	+50	0.1	8	6
		0.0	12	8
		-0.1	26	9
		-0.2	16	8
-15	-50	0.1	5	3
		0.0	9	3
		-0.1	10	5
		-0.2	collapsed	5
	0	0.1	12	3
		0.0	13	6
		-0.1	15	3
		-0.2	15	3
	+50	0.1	4	1
		0.0	10	3
		-0.1	12	6
		-0.2	12	3
-40	-50	0.1	3	4
		0.0	0	3
		-0.1	6	6
		-0.2	collapsed	2
	0	0.1	2	4
		0.0	4	3
		-0.1	4	5
		-0.2	3	3
	+50	0.1	8	2
		0.0	8	4
		-0.1	7	5
		-0.2	9	4

Table 5. Pitch imbalance through focus.

CONCLUSION

This study examined the lithographic abilities of a SCAA mask using 0.75 NA 193 nm lithography. Resolution down to a 140 nm pitch was achieved without phase imbalance or pitch walking. Pattern collapse was an issue which needs to be addressed. Some feature biasing was shown to be necessary in order to balance the chrome etch between the zero and pi spacing on the mask. However, little if any biasing looks to be necessary on the completed mask in order to balance the pitches of the resist features. These results suggest that a 65 nm dense pattern with a reasonable process window is possible using a 0.80 NA 193 nm scanner and optical extension techniques.

ACKNOWLEDGMENTS

The authors would like to acknowledge Kevin Poirier, Venu Vellanki and Patrick Reynolds of Benchmark Technologies for their contributions to this paper.

REFERENCES

1. M. Switkes, M. Rothschild, "Resolution Enhancement of 157 nm Lithography by Liquid Immersion," *SPIE*, 4691, pp. 459-465, 2002.
2. M. D. Levenson, J. S. Petersen, D. J. Gerold, C. A. Mack, "Phase Phirst! An improved strong-PSM paradigm," *SPIE*, 4186, pp. 395-404, 2001.
3. D. J. Gerold, J. S. Petersen, M. D. Levenson, "Multiple Pitch Transmission and Phase Analysis of Six Types of Strong Phase-Shifting Masks," *SPIE*, 4346, pp. 729-743, 2001.
4. J. Simons, D. Goldfarb, M. Angelopoulos, S. Messick, W. Moreau, C. Robinson, J. DePablo, P. Nealey, "Image Collapse Issues in Photoresist," *SPIE*, 4345, pp. 19-29, 2001.